GEOLOGICA CARPATHICA, JUNE 2018, 69, 3, 221–236 doi: 10.1515/geoca-2018-0013

Garavellite and associated sulphosalts from the Strieborná vein in the Rožňava ore field (Western Carpathians)

TOMÁŠ MIKUŠ[1, ✉], JULIAN KONDELA[2], STANISLAV JACKO[2] and STANISLAVA MILOVSKÁ[1]

[1]Earth Science Institute, Slovak Academy of Sciences, Ďumbierska 1, 974 01 Banská Bystrica, Slovakia; ✉mikus@savbb.sk
[2]Institute of Geosciences, Faculty of Mining, Ecology, Process Control and Geotechnologies, Technical University, Park Komenského 15, 042 00 Košice, Slovakia

(Manuscript received February 13, 2017; accepted in revised form March 15, 2018)

Abstract: The article presents the first description of a complete and continuous series from berthierite to garavellite sulphosalts in the Western Carpathians. Berthierite is a common main or accessory phase of Sb mineralizations in the Western Carpathians, and occurs at many localities and ore deposits as well. On the other side, garavellite or Bi-rich berthierite is a relatively rare accessory phase. The highest Bi content in garavellite reaches up to 38.04 wt. % which represents 0.90 apfu, and its crystallochemical formula can be written as $Fe_{0.97}Sb_{1.07}Bi_{0.90}S_{3.98}$. Raman band shifts were observed in the isomorphic berthierite–garavellite series. Garavellite occurs in the younger stages of sulphidic mineralization, and associates with tetrahedrite, berthierite, Bi-chalcostibite, Sb-bismuthinite, Bi-stibnite, ullmanite and cinnabarite. It creates irregular grains and veinlets in pre-existing tetrahedrite, or forms myrmekite intergrowths with chalcopyrite in tetrahedrite. Bi content in chalcostibite is up to 0.20 apfu. Besides the tetrahedrite, pre-existing sulphosalts are the members of the tintinaite–kobellite series, Bi-jamesonite and bournonite. The Sb/(Sb+Bi) ratio of minerals of the tintinaite–kobellite series varies from 0.37 to 0.80. The maximum content of Bi in jamesonite is up to 1.22 apfu. A vertical zonation at the ore vein body (mining levels 6/180 a.s.l., 8/80 a.s.l., 10/20 b.s.l.) is represented by the Sb decrease along with the Bi increase with increasing depth. Bi content continuously decreases during the older ore mineralization stage and Sb increases at the younger mineralization stage. Both of the stages have been enriched by Sb as well.

Keywords: garavellite, tintinaite–kobellite isoseries, Bi-sulphosalts, Micro-Raman spectroscopy, siderite–sulphidic mineralization, Strieborná vein deposit, Gemeric Superunit.

Introduction

Garavellite ($FeSbBiS_4$), in contrast to berthierite ($FeSb_2S_4$), is one of the rare minerals occurring in the ore deposits of the Western Carpathians. The rare mineral garavellite was first identified by Gregorio et al. (1979) in the Cu–Fe deposit of Valle del Frigido, Apuane Alps, Italy, in ore bodies composed of siderite with disseminated chalcopyrite. From the world occurrences, garavellite was also found in Pb–Zn deposits of Shaanxi (Wei et al. 1985), and more recently in Sn-base metal ore field of Dachang (Li et al. 1998) in China. Garavellite is also known from the Au-bearing quartz veins of the Kasejovice deposit in Czech Republic (Litochleb et al. 1990), and was found in Au-bearing quartz veins related to the shear zone of the Aprelkovskii deposit, Russia (Borovikov et al. 1990). Garavellite is reported from a historic sample from the Caspari mine (Germany) where garavellite is associated with berthierite, bismuthinite, chalcopyrite, and siderite (Bindi & Menchetti 2005). In Slovakia (Western Carpathians), garavellite is reported from the Sb–Au deposit in Pezinok (Andráš et al. 1993) and from the Mlynná dolina–Hviezda occurrences (Majzlan & Chovan 1997). Most recently, garavellite has been found in the Western Carpathians at the Klenovec–Medené locality within the quartz-sulphidic mineralization (Ferenc & Dzúrová 2015). Garavellite or Bi-rich berthierite associated with Bi sulphosalts occurs at the end of the sulphidic stage of the various types of mineralizations in the Western Carpathians: siderite–sulphidic, quartz–stibnite, and stockwork/disseminated.

Orthorhombic garavellite belongs to the berthierite isotype series (Bindi & Menchetti 2005; Moëlo et al. 2008) which includes also berthierite ($FeSb_2S_4$) and clerite ($MnSb_2S_4$). The atomic arrangement in the garavellite structure is topologically the same as in berthierite (Buerger & Hahn 1954; Lemoine et al. 1991; Lukaszewicz et al. 2001; Bindi & Menchetti 2005). The main building blocks of berthierite crystal structure are [SbS5] orthorhombic pyramids and [FeS6] octahedral; nevertheless, the non-ideal equality of inter-atomic distances and angles suggests slight distortion. One of two Sb positions (Sb2) of berthierite is increasingly occupied by Bi^{3+} up to 100 % in garavellite end-member (Gregorio et al. 1979; Bindi & Menchetti 2005), causing differences in the geometry, dimensions and constellation of coordination polyhedra.

This contribution is focused on the mineralogical and spectroscopic characterization of the garavellite–berthierite solid solution and associated Bi-sulphosalts from the Strieborná vein deposit, as well as on some paragenetic aspect.

The Raman spectra of berthierite and garavellite were previously published by Kharbish & Andráš (2014), and in

the public spectral database RRUFF (Lafuente et al. 2015). Kharbish & Andráš (2014) studied how crystal structure influences the number of the Raman bands, and discussed frequency shifts by the Sb2–Bi substitution. Here we are presenting the Raman spectra of these minerals along with a phase with an intermediate chemical composition, with an intention to identify equivalent Raman modes, and observe their wavenumber shift dependence on elemental substitutions.

Geological setting of the Strieborná vein

The Strieborná vein deposit of the Rožňava ore field (ROF) is situated at the south-eastern margin of the Western Carpathian basement units, inside the Gelnica Group formation of the Gemeric Superunit. The Early Paleozoic Gelnica Group forms the oldest sequence of the metasedimetary/metavolcanitic formations of the Gemeric Superunit. The ROF area is penetrated by the subparallely arranged hydrothermal siderite–sulphidic veins of SE–NW direction. The history of mining in the ROF started in the 13th century, when the greatest interest was focused mainly on gold (Eisele 1907), silver, copper (Schifter 1938; Pavlík 1967), antimony (Papp 1915) and mercury (Herčko 1971). In 1981, northwards from the Rožňava mining city, a new Strieborná vein was discovered near the Čučma village, and it became the most significant vein structure in the ROF. The vein position was compared with the historically known, parallely oriented Mária vein (Mesarčík 1994). The veins are situated in the NE–SW transpressive Transgemeric shear zone (Maťo & Sasvári 1997) where the Strieborná vein is divided into boudine structure, while the Maria vein is relatively solid. The distance between the Strieborná and Mária veins is 600 m (Fig. 1). The vein filling and the structural position in the ore field suggest a close link between the veins origin and structural evolution. The Strieborná vein genesis is the product of multiple

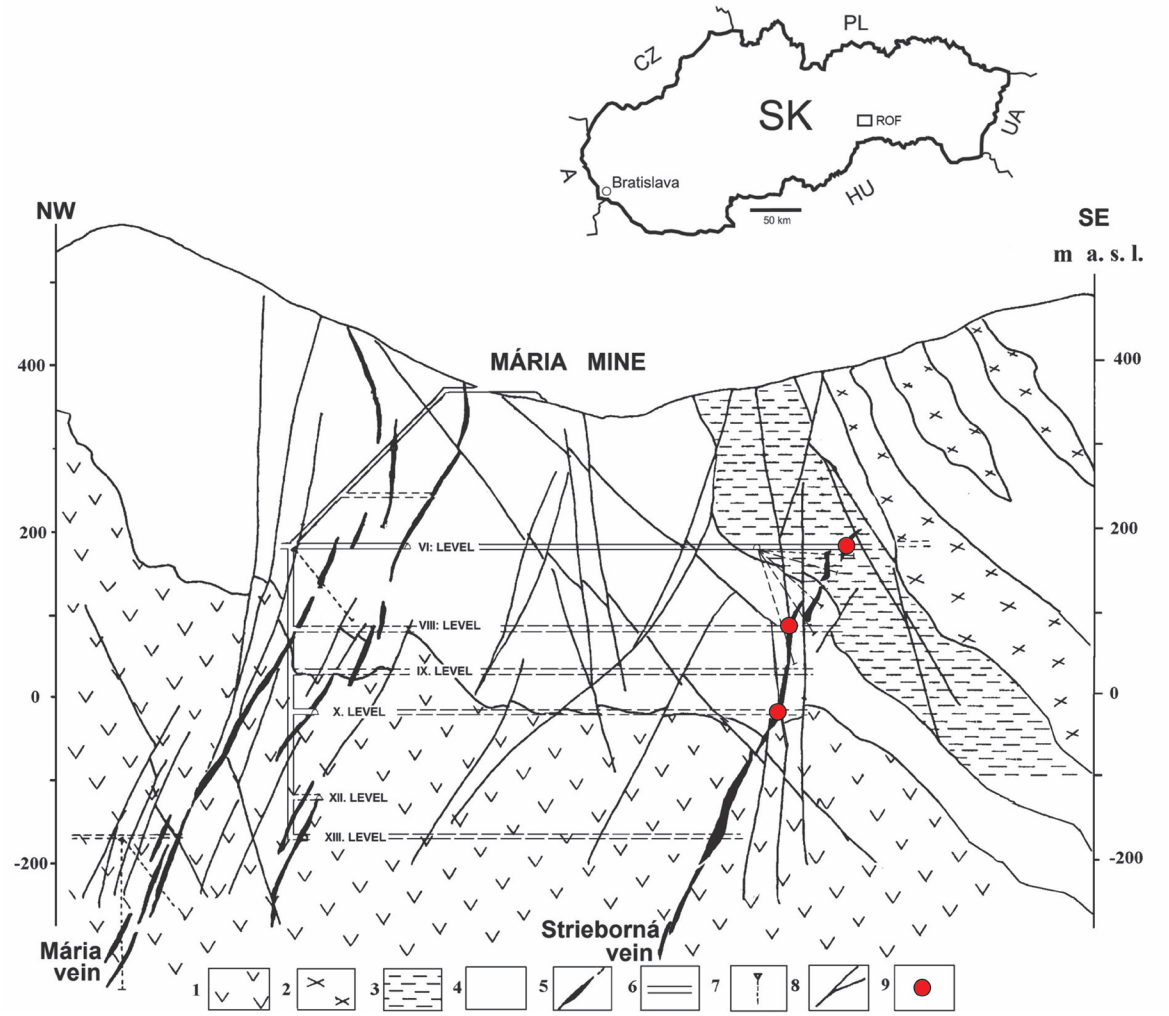

Fig. 1. Geological cross-section through the NE part of Rožňava–Mária ore segment (Mesarčík et al. 1991— modified). 1 — recrystallized metavolcanics (mafic pyroclastics); 2 — metasandstones interbedded by keratophyre metapyroclastics; 3 — altered grey metasandstones with black phyllite intercalations; 4 — coarse laminated metasandstones intercalated by green-grey phyllites; 5 — ore veins; 6 — mining levels; 7 — prospecting hole; 8 — faults; 9 — sampling location. The age of volcano-sedimentary complex is Late Paleozoic. The inset shows the location of the Rožňava ore field (ROF).

epigenetic hydrothermal mineralization (Sasvári & Maťo 1998; Hurai et al. 2002), with a close relationship between the vein filling and rheologically contrasting environment. Consequently, the vein does not crop out on the surface. The largest accumulation is known from the 10th mine horizon (20 m b.s.l.) in the total length of 1300 m. On this horizon, the veins have a NNE–SSW direction and general inclination 75–85° to the NNW, where the vein abruptly ends. The continuation of the vein gradually decays in the overlaying dark-black metapelites and grey metasandstones. Metaclasts often contain layers of quartz and lithic wackes. Below the 10th level (below 0 m a.s.l.) the ore body is situated within metasediments and metavolcanic rocks.

Mineralogy of the Strieborná vein

Major vein minerals are medium to the coarse-grained siderite of two generations and younger multi-generational quartz–sulphide mineralization of two generations. The most abundant ore minerals are tetrahedrite, chalcopyrite, pyrite and arsenopyrite. Brittle, steel-grey coloured tetrahedrite, which is the most important ore mineral, is spatially controlled by the older siderite that is in the form of reticulated veins and clusters. A more brittle tetrahedrite variety with steel blue colour and high metallic lustre is usually enriched by Cu, Ag, Bi, Sb and Hg. A darker low lustre variety contains more Zn and Fe (Sasvári & Maťo 1998). The high content of silver in tetrahedrite was the reason for the name of the Strieborná vein. The concentration of tetrahedrite in the vein bodies has a zonal distribution, and gradually decreases downwards to underlying rocks where it is substituted by pyrite (Mesarčík et al. 1991; Maťo & Sasvári 1997; Sasvári & Maťo 1998). Quartz is the main gangue mineral and forms several generations (Sasvári & Maťo 1998). The products of the youngest quartz–sulphide phase are tetrahedrite, kobellite, bismuthinite, bournonite, jamesonite and stibnite.

Methods

Samples for mineralogical study were collected in 1997 from the 8th and 10th mine horizons, and in 2015 from the 6th horizon (Fig. 1; Mária Mine — 48°40'35.3" N, 20°32'28.1" E). Polished samples were prepared for mineralogical and spectroscopic studies.

The chemical composition of sulphosalts was determined by using a wavelength-dispersive spectrometry (WDS) on an electron probe microanalyser (EPMA) JEOL JXA 8530FE (at the Earth Sciences Institute of the Slovak Academy of Sciences in Banská Bystrica) under the following conditions: accelerating voltage 20 kV, probe current 15 and 20 nA, beam diameter 2–3 μm, ZAF correction, counting time 20 s on peak, 10 s on background. For WDS analyses the following standards were used: X-ray lines and D.L. (in ppm): Ag(*Lα*, 45) — pure Ag, S(*Kα*, 26) — pyrite, Cu(*Kα*, 39) and Fe(*Kα*, 26) — chalcopyrite, As(*Lβ*, 208) — GaAs, Se(*Lβ*, 281) — Bi_2Se_3, Cd(*Lα*, 55) — CdTe, Sb(*Lα*, 47) — stibnite, Hg(*Mα*, 101) — cinnabar, Bi(*Lα*, 240) — Bi_2S_3, Pb(*Mα*, 93) — galena, Ni(*Kα*, 32) — gersdorffite, Co(*Kα*, 32) — pure Co, Zn (*Kα*, 45) — sphalerite.

The non-polarized Raman spectra were measured from berthierite and garavellite (polished sections) with the different content of Bi and Sb. We have used a LabRAM HR (Horiba Jobin-Yvon) microspectrometer with an Olympus BX41 microscope, and with confocally coupled Czerny-Turner type monochromator (focal length 800 mm). A laser emission at λ=632.8 nm (He–Ne laser) was used for excitation. The Raman scattered light was collected at 180° geometry through 100×/0.80 objective lens, and dispersed by a diffraction grating with the density of 600 gr.mm^{-1} onto a cooled CCD detector. The system resolution was 2 cm^{-1}, and the wavenumber accuracy was ±1 cm^{-1}. The grating turret accuracy was calibrated between a zero-order line (180° reflection) and laser line at 0 cm^{-1}. The spectral accuracy was verified on 734 cm^{-1} line of teflon. Measurement conditions were adjusted to achieve the best signal/noise ratio, and to prevent photochemical reactions (Makreski et al. 2013): laser power was dimmed to 0.054 mW on the sample surface (a level that was empirically found to be harmless to the sample), and this weak excitation power was compensated by long collection times. Each point was visually checked for thermal damage after the measurement. The spectra with high backgrounds were corrected by the subtraction of blank background record. The spectra were acquired in the range of 50–500 cm^{-1}, the exposition time was 6×500 s, using 6-fold sub-pixel shift. The positions of Raman lines were refined by peak fitting, using the Gaussian–Lorentzian function in the program PeakFit (SeaSolve Software Inc.). A factor group analysis was performed, using the tools of the Bilbao Crystallographic Server (www.cryst.ehu.es; Kroumova et al. 2003), using published crystallographic parameters for the studied minerals.

Results of the mineralogical research

Geological documentation

The Strieborná vein was discovered after drilling prospection in the 6th mine level (Fig.1). The studied part of the Strieborná vein mine gallery is localized in significantly foliated dark grey, thin-bedded metasandstones and black metapelites (Fig. 2). Surrounding rocks of the ore veins also contain subordinate pyrite and arsenopyrite involved in quartz veinlets. Idiomorphic pyrite grains are not jointed, and their size is up to 0.5 cm. Fine-grained arsenopyrite forms dark grey strips of up to 3 mm in thickness. Vein bodies are developed along foliation planes, and they are — like the host rocks — significantly tectonically affected**.** The Strieborná vein has NE–SW direction and shows SE steep inclination angle. The vein footwall is strictly cut by a fault, and the mine gallery vein thickness attains approximately 4.6 m (Fig. 2). Siderite is

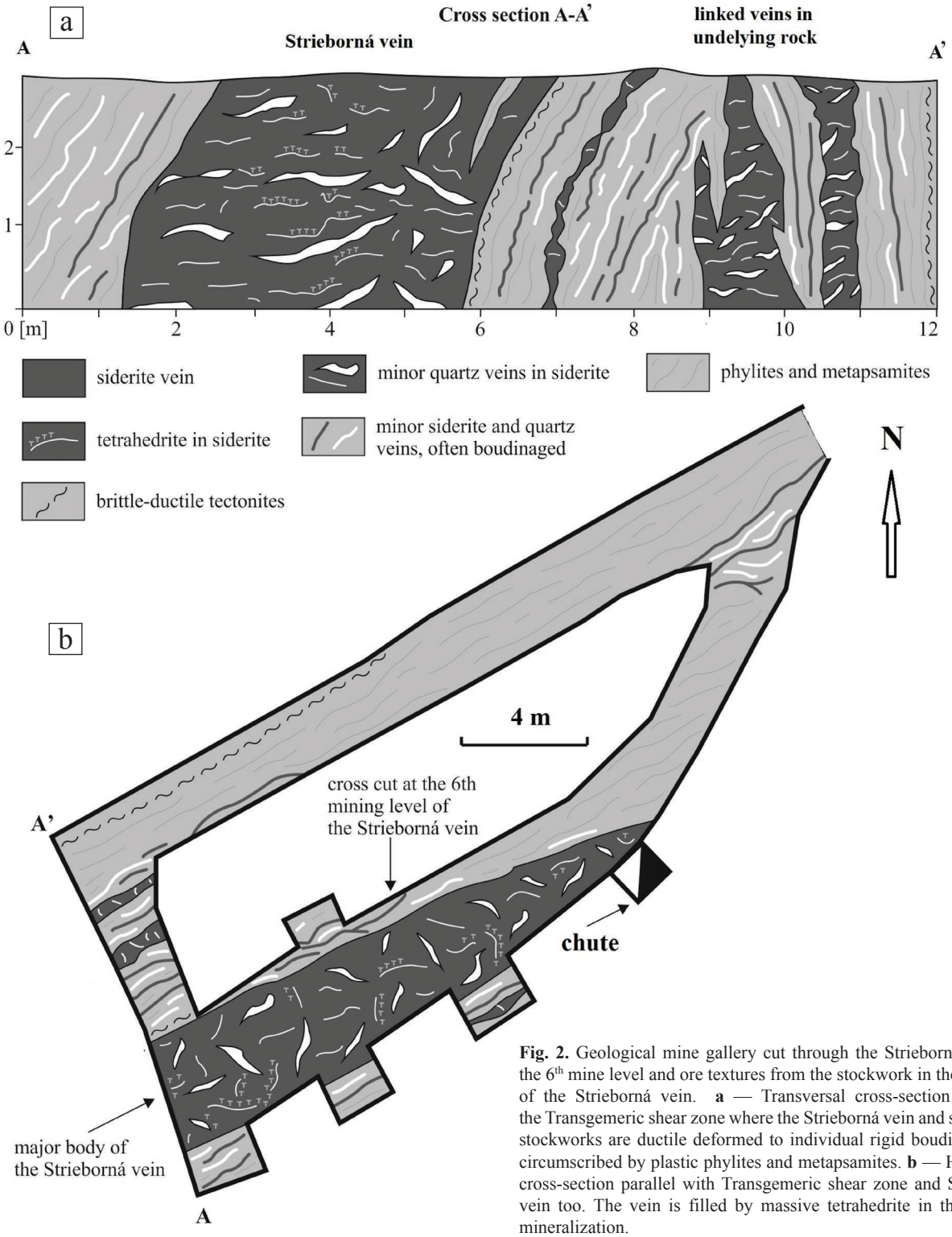

Fig. 2. Geological mine gallery cut through the Strieborná vein on the 6th mine level and ore textures from the stockwork in the footwall of the Strieborná vein. **a** — Transversal cross-section A–A´ in the Transgemeric shear zone where the Strieborná vein and subsidiary stockworks are ductile deformed to individual rigid boudine bodies circumscribed by plastic phylites and metapsamites. **b** — Horizontal cross-section parallel with Transgemeric shear zone and Strieborná vein too. The vein is filled by massive tetrahedrite in the siderite mineralization.

the major vein mineral, and it is intensively jointed and rarely brecciated. The second most abundant mineral of the vein is quartz. Along with tetrahedrite, it closes cracks in siderite, or fills nests and irregular veinlets. The tetrahedrite is the third most abundant mineral of the vein filling. It fills joints within the siderite body, or creates both thin veins and rare massive ore lenses (up to 0.5 m^2). At the 6th mine level of the Strieborná vein, tetrahedrite forms 3 textural types in siderite: stockworks, massive and breccia textures (Fig. 3). Pyrite and arsenopyrite are further macroscopically visible ore minerals of the vein infill. Pyrite grains having up to 1 cm dimensions show either irregular shapes or sizes, and they are also intensively jointed.

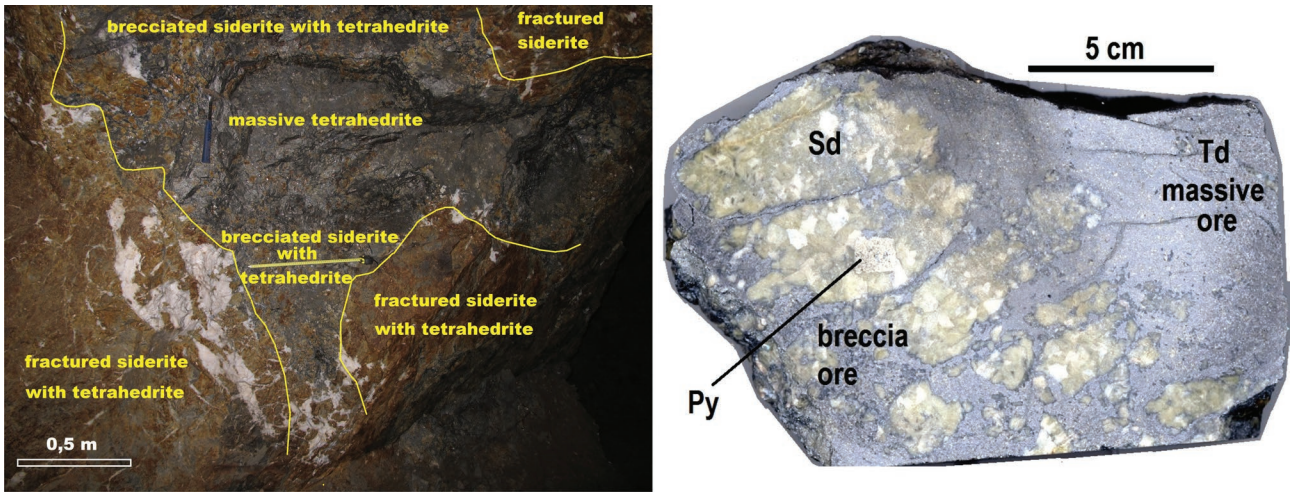

Fig. 3. Tetrahedrite textures from the Strieborná vein filling (6th mine level) showing transition from breccia to massive ore.

Paragenetic associations

Based on the detailed mineralogical study, several mineral associations of sulphosalts can be distinguished in the quartz–sulphidic stage of the Strieborná vein. The first older phases are represented by an association of tintinaite–kobellite series — Bi-jamesonite–bournonite–tetrahedrite (from oldest to youngest). The second one, the younger association than tetrahedrite, is represented by chalcostibite–berthierite–garavellite series — "horobetsuite" (Bi-stibnite, Sb-bismuthinite)–native Bi-stibnite. Considering the succession scheme of sulphosalts formation, the temporal decreases/increases of bismuth could be assumed for a period of sulphosalts evolution, namely the gradual decrease of Bi content in the fluids in the older stage, and its increase during the younger sulphosalts stage. The younger stage is also characteristic with Sb enrichment. Beside temporal relationships, spatial diversity could also be proposed in sulphosalts formation. In general, Sb content shows an apparently inverse depth proportional relationship (e.g., from the 6th to 10th mine level). Tetrahedrite content shows the same relationships, while Bi content increases at the same depth span. We have tried to outline and improve the succession scheme for the Strieborná vein as the result of our paragenetic study (Fig. 4). The proposed scheme also used data from Sasvári & Maťo (1998) and Dianiška (2013).

Berthierite $FeSb_2S_4$–Garavellite $FeSbBiS_4$ solid solution

Minerals of this series are relatively abundant, mainly at the 6th and 8th mine levels. They form several morphological types at the 6th mine level. Berthierite often associates with garavellite, forming a few mm. long veinlets or myrmekitic intergrowths with chalcopyrite in tetrahedrite. Berthierite creates intergrowths with chalcostibite and stibnite. Garavellite comprises up to 50 µm isometric grains, and associates with Bi-stibnite and Sb-bismuthinite in tetrahedrite. Hairline veinlets (Fig. 5c) formed by myrmekitic intergrowths of berthierite and chalcopyrite in tetrahedrite rarely contain garavellite and arsenopyrite (Fig. 5d). Occasional berthierite associates with ullmannite and cinnabar (Fig. 5b). At the 8th mine level garavellite often forms isometric grains up to 200 µm in tetrahedrite, where it is one of the most common sulphosalts associated with Sb-bismuthinite (Fig. 6d). Berthierite of the same mine level is fairly rare. The chemical heterogeneity of garavellite is a quite common feature. It often forms zones, which have an irregular shape, with diffuse interfaces in berthierite (Figs. 5d, 6d). Berthierite and garavellite are younger than tetrahedrite and chalcostibite but earlier than stibnite. The chemical composition of this series is represented by a continuous transition from a berthierite end member on the one side, to a garavellite end member on the other one (Fig. 7) through transition members — Bi-berthierite and Sb-garavellite. An empirical formula for berthierite (Bi-free) can be written as $Fe_{1.0}Sb_{1.98}S_{3.98}$ based on 7 apfu. Bi content and other measured elements in this type are negligible. $Bi^{3+} \rightarrow Sb^{3+}$ substitution in garavellite is intensive, showing a strong positive correlation (Fig. 7). Bi content continuously increases from 1.16 wt. % up to 38.04 wt. % which represents 0.02–0.91 apfu. Divalent cations are dominantly represented by Fe. Other elements are present only in minor amounts, except for Cu, which can reach up to 0.65 wt. %. An empirical formula for garavellite with the highest Bi content can be expressed as $Fe_{0.97}Sb_{1.06}Bi_{0.91}S_{4.01}$ based on 7 apfu. Representative microprobe analyses are presented in Table 1. With increasing depth, garavellite is more enriched in Bi and more abundant than berthierite (from 6th to 8th level). However, garavellite and berthierite were not found on the 10th mine level.

Based on the crystal symmetry and atomic coordinates of orthorhombic berthierite (Lukaszewicz et al. 2001) and garavellite (Bindi & Menchetti 2005), both of the spatial group *Pnam* (#62 — standard *Pnma)*, Z=4, our factor group analysis yielded a total of 42 Raman-active vibration modes (14Ag+7B1g+14B2g+7B3g). Not all of them are equally pronounced due to crystal orientation to the polarized laser beam.

Berthierite with 0.00 and 0.20 apfu of Bi, and garavellite with 0.89 apfu of Bi were chosen for the spectroscopic study (Table 1, Fig. 6d).

All Raman spectral peaks of berthierite, garavellite and the Bi-berthierite occur between 500–60 cm^{-1} (Fig. 8), their fitted values are listed in the Table 2. The dominant Raman peak of berthierite is centred at 268 cm^{-1}, other intense peaks are at 353, 278 and 58 cm^{-1}. Sharp bands occur in the region 110–58 cm^{-1}. The deconvolution of the spectrum yielded 25 significant bands (Table 2). The feature at 269 cm^{-1} dominates for the garavellite spectrum, the fitting resulted in 30 bands. The Bi-berthierite consists of 28 peaks and shows spectral similarities to both minerals (berthierite and garavellite). The strong berthierite band at 353 cm^{-1} tends to energy decrease towards garavellite (346 cm^{-1}); it has an asymmetric shape and is composed of three peaks (Table 2). With decreasing Bi content, the weak garavellite peak at 310 cm^{-1} progressively splits and grows into two stronger peaks at 304, 315 and 302, 317 cm^{-1} in Bi-berthierite and berthierite, respectively. The dominant band centred at 268 cm^{-1} has virtually no shift towards garavellite; however, it broadens and splits into at least to two peaks. The berthierite Raman band at 258 cm^{-1} is probably incorporated into a broad peak at 269 cm^{-1} in the garavellite spectrum. Both, the evolution of the medium and low intensity peaks in the spectral region between 250 and 110 cm^{-1} are unclear. The wavenumber position of features at 104 and 95 cm^{-1} is changing towards lower frequencies with increasing Bi content, and bands at 80 and 74 cm^{-1} seam to transform to a broad weak band at 77 cm^{-1}.

The broad shape of dominant peaks of expected internal modes are typical for all spectra phases in the region. Despite distinct shifts between some peaks in berthierite and garavellite, their equivalence may be clearly traced through the Bi-berthierite spectrum (Table 2).

Associated sulphosalts

Jamesonite $FePb_4Sb_6S_{14}$

It occurs rarely in studied samples and forms needle aggregates up to 0.5 mm. On the 6th mine level, jamesonite is associated with older tintinaite, and is corroded by later tetrahedrite, bournonite, bismuthinite and native Bi (Fig. 6a,b). Bi content is up to 7.98 wt. % that corresponds to 0.83 apfu. Bi/(Bi+Sb) ratio (0.095) is less than in tintinaite (0.335), and at the same time higher than in bournonite (0.017) and tetrahedrite (0.008). This could suggest the consistent regress of Bi concentration in fluids during the crystallization of sulphosalts in the following succession: tintinaite–jamesonite–bournonite–tetrahedrite. This succession is also obvious from microscopic observations. Other elements are present only in minor amounts. Electron microanalyses are presented in the Table 3. An empirical formula for jamesonite can be written as $Fe_{0.95}Pb_{4.02}(Sb_{5.35}Bi_{0.56})_{5.91}S_{14.00}$ based on 25 apfu. Bi-rich jamesonite is associated with tintinaite and bournonite. It occurs only rarely at the 10th mine level, and contains up to 11.78 wt. % of Bi (1.22 apfu) (Table 3). Cu content is relatively high (0.29 apfu) and probably partly substitutes Fe. This idea is supported by a negative correlation trend between Cu and Fe. Its empirical formula, based on of 25 apfu, can be written as $Fe_{0.85}Cu_{0.29}Pb_{3.95}(Sb_{4.76}Bi_{1.22})_{5.98}S_{13.91}$.

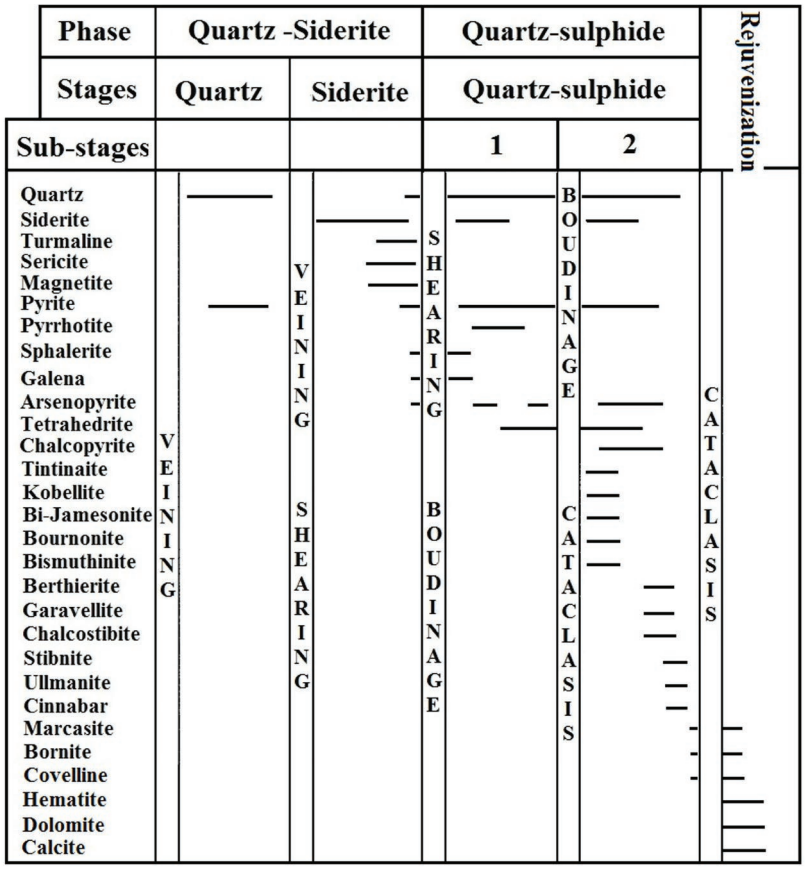

Fig. 4. Succession scheme of the hydrothermal mineralization in the Strieborná vein. The scheme is proposed based on this study and published data of Sasvári & Mať o (1998) and Dianiška (2013).

Bournonite $CuPbSbS_3$

It was found in all three studied mine levels. It usually forms xenomorphous grains up to 0.1 mm. At the 6th level, bournonite intensively corroded tintinaite via cracks and cleavage planes (Fig. 6b), and also corroded jamesonite needles (Fig. 6a). The Bi content is up to 3.24 wt. % (0.08 apfu) which is characteristic for interstitial grains between tintinaite and jamesonite. Locally, high Bi

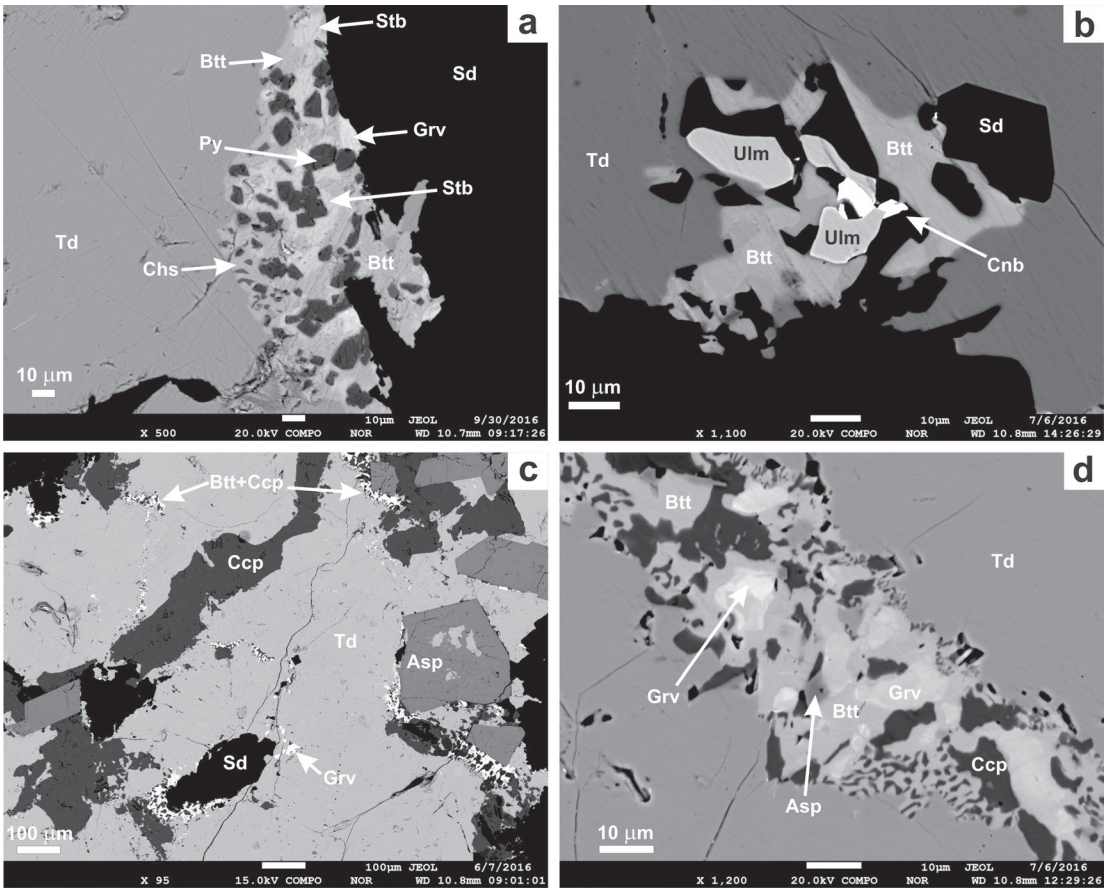

Fig. 5. a — BSE images of berthierite (Btt) and garavellite (Grv) associated with chalcostibite (Chs) and stibnite (Stb) replacing tetrahedrite (Td) grain from the margin. Tetrahedrite is associated with siderite (Sd). **b** — Bi-berthierite associated with ulmanite (Ulm) and cinnabarite in tetrahedrite with siderite (Sd). **c** — Veinlets of berthierite–chalcopyrite myrmekites in tetrahedrite. **d** — Myrmekitic intergrowth of berthierite (Btt) with chalcopyrite (Ccp). Berthierite contains garavellite (Grv) grains with diffusional margins.

contents in bournonite could be the result of reaction between fluids and older Bi-sulphosalts. Other measured elements are present only in low concentrations (Table 4). At the 10th mine level, bournonite intensively corroded kobellite, and rarely associates with younger Sb-bismuthinite. It forms needle crystals up to 0.5 mm.

Kobellite–tintinaite (Cu, Fe)$_2$Pb$_{10}$(Sb, Bi)$_{16}$S$_{35}$ series N=2

Sulphosalts of this series represent the most common ones in the deposit. They were found at the 6th and 10th mine levels. At the 6th mine level, tintinaite forms needle crystals up to several cm in size. It occurs in association with jamesonite (Fig. 6a), tetrahedrite, bournonite, bismuthinite and native Bi (Fig. 6b). Tintinaite represents the oldest sulphosalt. Its cleavage planes and cracks are rejuvenated by bournonite and native Bi. At the10th mine level, the kobellite is associated and intensively corroded with younger bournonite, Sb-bismuthinite and Bi-jamesonite. In general, with increasing depth, an increase of Bi and a decrease of Sb are observed. Sb-rich members of the 6th mine level can be considered as tintinaite and Bi-rich members at the 10th mine level as kobellite (Fig. 9). Paradoxically, the highest Bi content occurs in kobellite which forms isometric grains (up to 20 μm) in tintinaite found at the 6th mine level. Antimony content in members of this series ranges between 5.84 up to 12.96 apfu. Bismuth content varies from 3.18 to 9.78 apfu. The Bi–Sb substitutional trend seems to be ideal (Fig. 9). Sb/(Sb+Bi) ratio varies from 0.37 to 0.80 (Fig. 10). Silver content is only minor (in average 0.06 apfu). Fe+Cu content in the studied phases is higher than that reported for the kobellite-tintinaite series (Fe+Cu=2 apfu, Zakrzewski & Makovicky 1986). The maximum content of Cu+Fe is 3.12, 2.22 in average. Cu content in many studied samples exceeds 2 apfu (maximum 2.23). Among the minor elements, only Hg is slightly increased (up to 0.86 wt. %). An empirical formula for tintinaite with the highest Sb content (and assuming cation substitutions) can be written as $(Cu_{1.92}Fe_{0.08})_2$ $(Cu_{0.24}Ag_{0.08}Hg_{0.1}Pb_{9.89})(Sb_{12.85}Bi_{3.16})S_{34.67}$ with chemically calculated N=1.97. An empirical formula for kobellite with the highest Bi content can be written as $(Cu_{1.59}Fe_{0.41})_2(Cu_{0.11}Pb_{10.31}Bi_{9.78}Sb_{5.84})S_{34.90}$ with calculated N=1.99 (Table 5).

Tetrahedrite (Cu, Ag)$_{10}$(Fe, Zn...)$_2$(Sb, As...)$_4$(S, Se)$_{13}$

Tetrahedrite is one of the most abundant ore minerals of the Strieborná vein. It forms xenomorphous aggregates up to

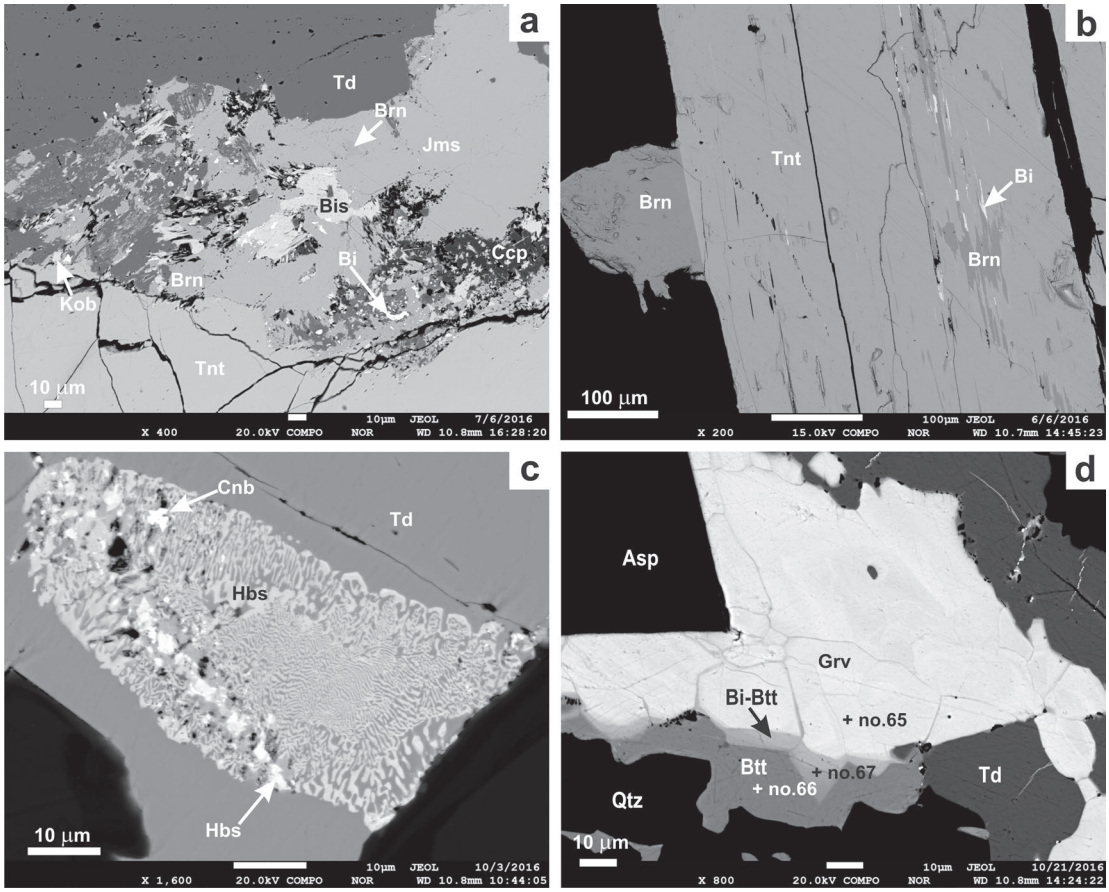

Fig. 6. a — BSE images of tintinaite (Tnt) associated with jamesonite (Jms), bournonite (Brn), bismuthinite (Bis), kobellite (Kob) and native Bi (Bi) are corroded by tetrahedrite (Td) and chalcopyrite (Ccp). **b** — Needle-shaped tintinaite crystal (Tnt) is replaced by bournonite (Brn) and native bismuth (Bi). **c** — Exsoluted "horobetsuite" grain (Hbs) in tetrahedrite (Td) is associated with cinnabarite (Cnb). **d** — Garavellite (Grv), Bi-berthierite (Bi-Btt) and berthierite (Btt) are associated with arsenopyrite (Asp) and replacing tetrahedrite (Td). Points from EPMA measurements were used for micro-Raman study. WDS analyses are given in Table 1.

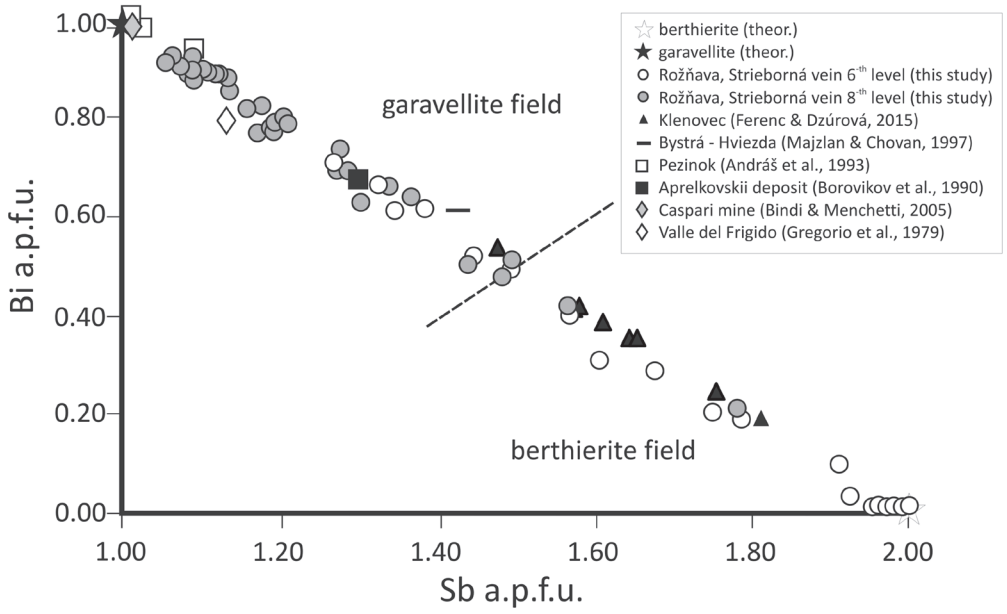

Fig. 7. Sb vs. Bi (apfu) graph for studied members of the berthierite–garavellite solid solution from the Strieborná vein, compared with some other published data from their occurrences in the Western Carpathians and in the world.

several cm in size. Tetrahedrite is corroded by an older sulphosalt association, represented by tintinaite, jamesonite and bournonite on the 6th level. Tetrahedrite grains are intensively corroded by chalcostibite, stibnite, berthierite–garavellite (Fig. 5a) and myrmekites of Sb-bismuthinite (Fig. 6c). Cracks or veinlets in tetrahedrite are often filled with myrmekites of berthierite–garavellite, chalcopyrite and arsenopyrite (Fig. 5c, d) as well as cinnabar. The crystallochemical formula of tetrahedrite was calculated according to Moëlo et al. (2008), as $^{[III]}A_6{}^{[IV]}(B,C)_6{}^{[III]}X_4{}^{[IV]}Y_{12}{}^{[VI]}Z_1$, where A=Cu, Ag; B=Cu, Ag and C is a generally divalent metal (Fe, Zn, Hg, Cd etc.) in the same coordination as B; X=Sb, As, Bi, Te; Y and Z=S and Se. The analysed tetrahedrite has quite a simple composition. The A site is dominantly occupied by Cu. Silver content reaches up to 0.27 apfu (1.72 wt. %). The B site is fully occupied by copper. The divalent C position is occupied mainly by Fe (up to 1.8 apfu), Zn (up to 0.34 apfu), and minor Hg (up to 0.16 apfu) and Cd (up to 0.02 apfu). The X position is dominantly occupied by Sb, and only minor contents of As (up to 0.63 apfu) and Bi (up to 0.03 apfu) are present. The overall occupation of the X site (Sb+As+Bi) varies from 3.96 to 4.17 apfu with a mean of 4.05 apfu. The Y and Z sites are fully occupied by sulphur. Se content is only minor and reaches up to 0.02 apfu. The average Se content from 90 analyses is zero. The empirical average (90 analyses, Table 6) chemical formula of the studied tetrahedrite can be written as: $(Cu_{5.86}Ag_{0.14})_{\Sigma 6.00}$ $Cu_{4.03}(Fe_{1.66}Zn_{0.22}Hg_{0.1}Cd_{0.01})_{\Sigma 1.99}(Sb_{3.91}As_{0.14}Bi_{0.01})_{\Sigma 4.05}S_{12.95}$, based on 29 apfu.

Table 1: Electron microprobe analyses of berthierite–garavellite solid solution. Analyses no. 66, 67 and 65 represent phases measured with micro-Raman spectroscopy (see Fig. 5d). H.no. — horizon number.

Sample	h.no.	Fe	Sb	As	Bi	Cu	S	Zn	Pb	Total
J-2 (66)	**8**	12.69	56.71	0.06	0.00	0.20	29.95	0.01	0.04	99.68
RV 2750	6	13.02	56.20	0.05	0.11	0.06	30.60	0.06	0.03	100.13
1 RV-Z-2	6	13.19	54.17	0.01	1.16	0.37	29.62	0.03	0.02	98.56
RV 2750	6	12.61	52.70	0.07	4.10	0.27	29.07	0.03	0.07	98.92
1 RV-Z-2	6	12.74	48.96	0	8.32	0.19	28.88	0.02	0.02	99.13
J-2 (67)	**8**	12.15	48.23	0.07	9.14	0.18	28.68	0	0.07	98.51
1 RV-Z-2	6	12.37	45.62	0.03	12.83	0.40	28.33	0.04	0	99.61
RV 2750	6	12.31	43.89	0.04	14.02	0.39	28.30	0	0.05	99.00
5 RV-5 SOS	6	12.01	41.76	0.07	17.83	0.38	27.76	0.08	0.25	99.94
RV 2750	6	11.62	37.52	0.03	22.68	0.13	27.19	0.01	0.06	99.24
1 RV-Z-2	6	11.56	34.98	0.01	26.18	0.25	26.65	0.03	0.03	99.68
1 RV-Z-2	6	11.40	33.40	0.01	28.27	0.36	26.46	0.02	0.12	100.02
RV 2750	6	11.30	31.81	0	30.15	0.46	26.37	0	0	100.08
J-2	8	10.92	26.41	0.02	36.86	0.37	25.41	0.05	0.17	100.20
J-2 (65)	8	10.91	26.75	0.08	37.13	0.14	25.64	0.04	0.13	100.82
J-2	8	10.84	26.30	0	37.29	0.92	25.42	0.03	0.13	100.64
J-2	8	11.08	25.77	0.02	38.04	0.48	25.40	0.02	0.20	101.00
Formula calculated to sum Fe+Sb+Bi=3										
J-2 (66)	8	0.98	2.00	0.00	0.00	0.01	4.01	0.00	0.00	
RV 2750	6	0.99	1.96	0.00	0.00	0.00	4.04	0.00	0.00	
1 RV-Z-2	6	1.02	1.93	0.00	0.02	0.03	4.00	0.00	0.00	
RV 2750	6	0.99	1.91	0.00	0.09	0.02	3.99	0.00	0.00	
1 RV-Z-2	6	1.01	1.79	0.00	0.18	0.01	4.01	0.00	0.00	
J-2 (67)	8	0.98	1.78	0.00	0.20	0.01	4.02	0.00	0.00	
1 RV-Z-2	6	1.00	1.69	0.00	0.28	0.03	3.99	0.00	0.00	
RV 2750	6	1.00	1.64	0.00	0.31	0.03	4.01	0.00	0.00	
5 RV-5 SOS	6	0.99	1.58	0.00	0.39	0.03	3.99	0.01	0.00	
RV 2750	6	0.99	1.46	0.00	0.51	0.01	4.02	0.00	0.00	
1 RV-Z-2	6	1.00	1.38	0.00	0.60	0.02	4.00	0.00	0.00	
1 RV-Z-2	6	0.99	1.33	0.00	0.66	0.03	4.00	0.00	0.00	
RV 2750	6	0.98	1.27	0.00	0.70	0.04	4.00	0.00	0.00	
J-2	8	0.98	1.09	0.00	0.89	0.03	3.99	0.00	0.00	
J-2 (65)	8	0.98	1.10	0.01	0.89	0.01	4.01	0.00	0.00	
J-2	8	0.97	1.07	0.00	0.90	0.07	3.98	0.00	0.00	
J-2	8	1.00	1.06	0.00	0.91	0.04	3.98	0.00	0.00	

Chalcostibite $CuSbS_2$

Chalcostibite occurs mainly on the 6th mine level as an accessory and phase associate with berthierite and stibnite (Fig. 5a). It forms up to 10 μm xenomorphous aggregates and rims on tetrahedrite grains. Chalcostibite is corroded by stibnite (Fig. 5a). The chemical composition shows increased content of Bi up to 0.03 apfu (2.36 wt. %). Higher Bi contents are observed in chalcostibite, associated with Bi-berthierite. Iron content can be slightly increased (up to 0.04 apfu) as well. The content of other elements is only minor (Table 7). At the 8th mine level, only sporadic Bi-chalcostibite was found, likely as a product of breakdown of Bi-rich sulphosalts. It forms myrmekitic overgrowth with Sb-bismuthinite in tetrahedrite. Sb is substituted by Bi in chalcostibite, and Bi content reaches up to 0.20 apfu (15.46 wt. %). The chemical formula of Bi-chalcostibite can be written as $Cu_{1.01}(Sb_{0.80}Bi_{0.20})S_{1.98}$ (Table 7). Chalcostibite was not found on the 10th mine level.

Stibnite Sb_2S_3–bismuthinite Bi_2S_3 solid solution

Both end-members (stibnite and bismuthinite) were found at the Strieborná vein as well as transition members Bi-stibnite and Sb-bismuthinite, formerly known as "horobetsuite". Stibnite and bismuthinite form isometric grains up to 50 μm in size. Bi-stibnite and Sb-bismuthinite are common minerals forming myrmekitic intergrowths and exsolutions in tetrahedrite up to 100 μm (Fig. 6c), or isometric grains in tetrahedrite and stibnite. Stibnite is younger than chalcostibite and berthierite (Fig. 5a). Bismuthinite replaces jamesonite and tetrahedrite (Fig. 6a). Stibnite was found only on

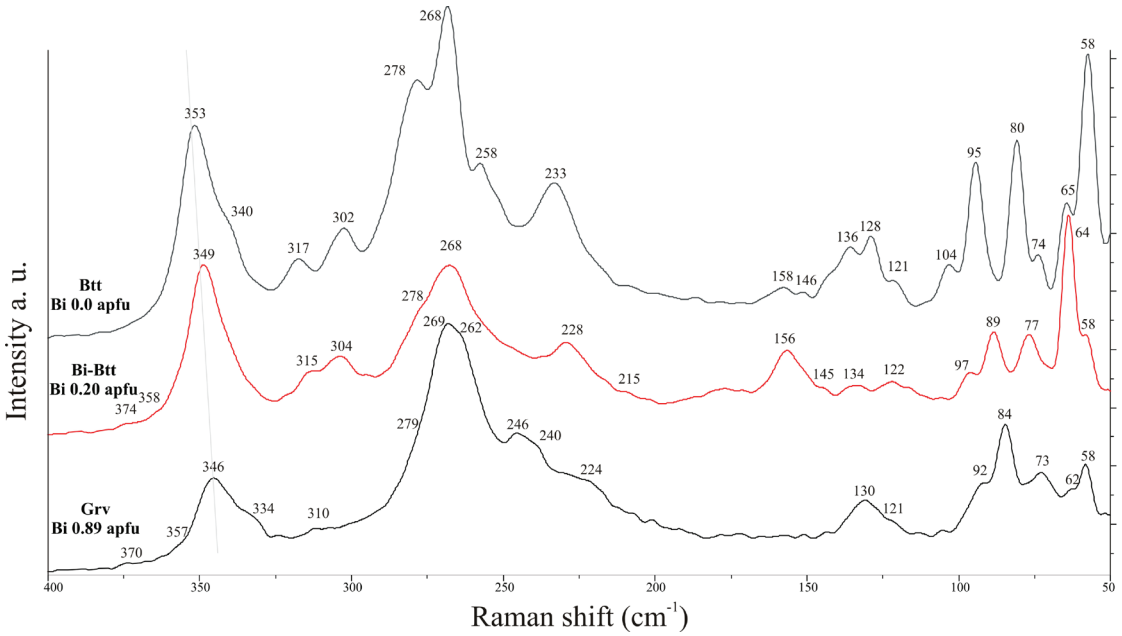

Fig. 8. Raman spectra of berthierite (Btt) — Bi free, Bi-berthierite — Bi 0.2 apfu and garavellite (Grv) — 0.89 apfu from the Strieborná vein. a. u. — arbitrary unit. Main Raman bands are labelled.

berthierite Bi — 0.00 *apfu*			**Bi-berthierite** Bi — 0.20 *apfu*			**garavellite** Bi — 0.89 *apfu*		
Band position cm^{-1}	FWHM cm^{-1}	I	Band position cm^{-1}	FWHM cm^{-1}	I	Band position cm^{-1}	FWHM cm^{-1}	I
58	4	62	58	5	37	58	4	49
65	5	38	**64**	**4**	**100**	62	5	31
74	5	20	77	10	44	66	6	21
80	3	44	89	7	44	73	6	32
95	4	50	97	7	19	84	6	64
104	5	16	106	10	13	92	5	23
110	11	5	115	3	7	97	7	17
121	7	13	122	12	19	105	10	4
128	3	22	134	14	19	113	12	21
136	7	21	145	9	5	121	7	15
142	6	11	156	16	40	130	13	38
146	5	5	177	18	15	147	17	15
158	12	8	215	43	16	159	17	16
186	6	5	228	17	28	175	18	17
233	19	40	252	28	28	190	17	15
253	13	25	256	2	2	203	21	20
258	4	16	267	17	57	224	23	40
268	**11**	**100**	273	13	23	240	14	33
278	10	53	278	2	4	246	11	32
283	9	31	281	14	24	254	10	14
302	9	28	294	10	7	262	13	43
317	9	19	304	15	30	**269**	**18**	**100**
340	9	17	315	10	15	279	31	21
347	11	20	322	2	3	310	31	16
353	10	62	342	19	30	324	2	2
			349	11	67	334	12	22
			358	7	2	339	8	11
			374	5	1	346	11	41
						357	12	8
						370	33	6

Table 2: Raman band positions of berthierite, Bi-berthierite and garavellite. FWHM — Full width at half maximum; I — normalized intensity in %.

the 6th mine level. Sb-bismuthinite is dominantly associated with garavellite in tetrahedrite on the 8th mine level. Deeper, on the 10th level, it occurs only rarely and replaces earlier kobellite. The chemical composition of stibnite is simple, with slightly increased Fe (up to 0.59 wt. %) and Cu (up to 1.13 wt. %) contents. Cu excess can be caused by the contamination by chalcostibite intergrowths. Other elements are present only in minor volumes (Table 8). Sb content in Sb-bismuthinite (Fig. 11) ranges from 4.3 to 29.5 wt. % (0.17–0.99 apfu). Bi content in Bi-stibnite ranges between 8.17–48.62 wt. % (0.14–0.95 apfu). The Sb/Bi substitution trend is shown in the Fig. 11. Some Bi-stibnite and Sb-bismuthinite contain increased amounts of Fe (up to 1.65 wt. %) and Cu (up to 1.8 wt. %). Cu positively correlates with Bi and Sb contents.

Ullmannite NiSbS

Ullmannite is only a rare minor phase. On the 6th mine level, it associates with tetrahedrite, Bi-berthierite and cinnabar.

Table 3: Electron microprobe analyses of Bi bearing jamesonite. H.no. — horizon number.

Sample	h.no.	Fe	Sb	As	Bi	Cu	S	Zn	Pb	Total
4 RV-Z-1	6	2.49	30.89	0	4.94	0.29	21.11	0	39.32	99.04
4 RV-Z-1	6	2.53	31.41	0.04	4.47	0.29	21.02	0.04	38.97	98.79
4 RV-Z-1	6	2.49	29.13	0.08	7.45	0.19	20.87	0.01	38.82	99.02
4 RV-Z-1	6	2.40	28.86	0.05	7.98	0.25	20.61	0.02	38.22	98.40
4 RV-Z-1	6	2.54	31.44	0	3.30	0.24	21.10	0.04	39.44	98.10
4 RV-Z-1	6	2.50	31.46	0.04	3.95	0.51	21.13	0.03	39.04	98.65
4 RV-Z-1	6	2.40	29.89	0.04	6.25	0.32	21.12	0.05	39.22	99.29
108-4466	10	2.19	26.84	0.09	11.78	0.86	20.64	0	37.86	100.27
108-4466	10	2.10	25.90	0.02	12.71	1.90	20.69	0.05	36.82	100.19
Formula based on 11 cations										
4 RV-Z-1	6	0.95	5.40	0.00	0.50	0.10	14.01	0.00	4.04	
4 RV-Z-1	6	0.97	5.49	0.01	0.46	0.10	13.96	0.01	4.00	
4 RV-Z-1	6	0.96	5.15	0.02	0.77	0.06	14.00	0.00	4.03	
4 RV-Z-1	6	0.94	5.15	0.01	0.83	0.08	13.97	0.01	4.01	
4 RV-Z-1	6	0.97	5.51	0.00	0.34	0.08	14.04	0.01	4.06	
4 RV-Z-1	6	0.95	5.48	0.01	0.40	0.17	13.98	0.01	4.00	
4 RV-Z-1	6	0.91	5.24	0.01	0.64	0.11	14.04	0.02	4.04	
108-4466	10	0.85	4.76	0.03	1.22	0.29	13.91	0.00	3.95	
108-4466	10	0.81	4.57	0.01	1.31	0.64	13.85	0.02	3.81	

Table 4: Electron microprobe analyses of bournonite (*n* is average of 28 analyses). H.no. — horizon number.

Sample	h.no.	Sb	Hg	As	Bi	Cu	S	Cd	Pb	Total
RV 2753	6	23.97	0	0	0	13.29	19.77	0.11	43.48	100.61
RV 2753	6	22.32	0.24	0	3.24	12.29	19.56	0	42.32	99.96
RV 2753	6	23.19	0.01	0.08	0.80	12.95	19.37	0	42.93	99.32
RV 2753	6	24.77	0	0.02	0	13.46	19.70	0.15	42.09	100.19
4 RV-Z-1	6	25.11	0.15	0.04	0	13.60	19.98	0	41.14	99.47
n=28		*23.93*	*0.03*	*0.07*	*0.43*	*13.38*	*19.63*	*0.06*	*42.50*	*100.05*
Formula calculated to sum Sb+Cu+Bi+Pb=3										
RV 2753	6	0.96	0	0	0	1.02	3.00	0.00	1.02	
RV 2753	6	0.91	0.01	0	0.08	0.96	3.03	0	1.01	
RV 2753	6	0.94	0.00	0.01	0.02	1.01	2.99	0	1.03	
RV 2753	6	0.99	0	0.00	0	1.03	2.98	0.01	0.99	
4 RV-Z-1	6	1.00	0.00	0.00	0	1.00	3.02	0	0.96	
n=28		*0.96*	*0.00*	*0.00*	*0.01*	*1.03*	*2.99*	*0.00*	*1.00*	

It is more abundant on the 8th mine level where it associates with chalcopyrite, chalcostibite and tetrahedrite. Ullmannite forms isometric grains up to 200 µm. It often overgrowths with tetrahedrite. Ullmannite was not found on the 10th mine level. It shows small contents of Fe (up to 0.05 apfu) and As (up to 0.04 apfu) (Table 9).

Discussion

The mineralogical research of the polystadial Strieborná vein sulphosalts allows us to understand the berthierite to garavellite transition mode in the vertical course of the Strieborná ore vein. The vein's evolution closely relates to the Transgemeric shear zone (TGS) which has also participated in the incoherent structure of the Western Carpathians during paleo-Alpine (Cretaceous) evolution (Lexa et al. 2003). The tectonometamorphic processes in the shear zone are responsible for the formation of some mineralization stages (Mesarčík et al. 1991) and they are also responsible for later boudinal destructions of the ore veins.

The Strieborná vein ore bodies have been observed on different mining levels (6/180 a.s.l., 8/80 a.s.l., 10/20 b.s.l.). The research results have confirmed the vertical zonality of sulphosalts including berthierite to garavellite transition (cf. Fig. 8) for first time in the Western Carpathians. The chemical composition of berthierite–garavellite solid-solution from the Strieborná vein is the most complex compared to published data worldwide (Fig. 7).

We have tried to compare the spatial zonation of the Strieborná vein sulphosalts with other world occurrences of similar sulphosalts in shear zones, however this was not possible, as the published data come from single spots in each of the studied localities (e.g., Orlandi et al. 2010; Ferenc & Dzúrová 2015). Some other data come from mine waste (Kharbis & Andráš 2014; Uher et al. 2000), others belong to a historical collection (Bindi & Mencheti 2005), represent experimental analysis products (Liu et al. 2008) or belong to a skarn occurrence (Ciobanu et al. 2014). The sulphosalts represent a genetically well-defined group evolved in specific conditions of hydrothermal processes. The temperatures controlling the substitution of extended solid solution of sulphosalts vary from 300 to 400 °C (Moëlo et al. 2008).

Our Raman spectra are basically similar to those of Kharbish & Andráš (2014) and results of the RRUFF database (Lafuente et al. 2015), though they show significant differences in the relative intensities of several bands. Since neither our nor their spectra were excited by a depolarized beam, some modes may be suppressed while others are enhanced, depending on a crystal orientation. Our fitting yielded more peaks than were recognized by Kharbish & Andráš (2014), who omitted several shoulders that are clearly pronounced in our spectra as distinct peaks. Large discrepancies in the intensities of presumably equivalent vibrations in their spectra are likely caused by the different crystal orientation to the incident beam. In addition, our samples represent syntaxially grown zones (optical observations), thus the spectra are similar, and corresponding vibrational modes are believed to be equally pronounced.

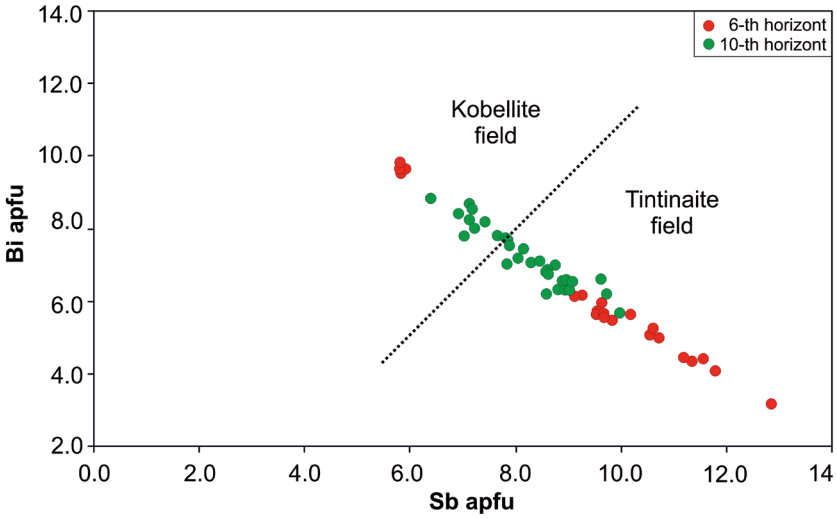

Fig. 9. Sb vs. Bi (apfu) plot for tintinaite–kobellite series from the Strieborná vein. Dashed line represents a formal border between kobellite and tintinaite.

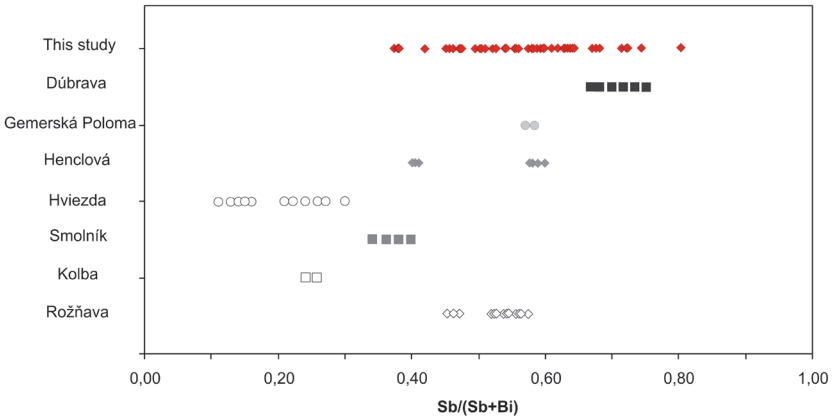

Fig. 10. Comparison of Sb/(Sb+Bi) (in apfu) ratios of kobellite–tintinaite series minerals from the Strieborná vein in the Rožňava ore field with other occurrences in the Western Carpathians (hydrothermal Sb-Au mineralization, siderite–sulphidic and massive sulphide deposits). Data from Kupčík et al. (1969), Chovan et al. (1998), Majzlan & Chovan (1997), Pršek & Mikuš (2006) and Klimko et al. (2009).

For instance, in our berthierite spectrum we recognized five distinct bands in the region of 110–60 cm^{-1}, while in the spectrum of Kharbish & Andráš (2014), five bands are visible, but only three of them were fitted. In the region 355–330 cm^{-1}, we have found 3 bands instead of the two of the former authors. Their relative peak intensities of garavellite also differ from ours. The most striking is missing of their dominant band at 214 cm^{-1} in our spectra, while others are amplified. The spectra of garavellite and berthierite of this study show similar band shapes, and accordance between equivalent peaks is even more apparent if "linked" through the Bi-berthierite with its intermediate band frequencies. According to Wang et al. (1994), Kharbish & Andráš (2014), the stretching and bending vibrations of sulphides are expected at 500–200 cm^{-1}. The 160–60 cm^{-1} features in the region could be assigned to lattice modes. Kharbish & Andráš (2014) tentatively attributed spectral band at 347 cm^{-1} in berthierite to the symmetrical stretching of Sb–S. The band at 347 cm^{-1} in our spectra causes an asymmetry of broad band centred at 353 cm^{-1}. The shoulder at 340 cm^{-1} could be then assigned to the antisymmetrical stretching of Sb–S.

Bismuth substitution for Sb2 in garavellite affects also the length of Sb–S bands in polyhedra — Sb–S distances shortened from 2.716 Å of $(Sb1–S)_{ber}$ to 2.678 Å of $(Sb1–S)_{gar}$ (Bindi & Menchetti 2005), resulting in the upshift of vibrational frequencies (Kharbish & Andráš 2014). In our spectra, this effect may be pronounced by the separation of weak peaks at 358 and 374 cm^{-1} in Bi-berthierite, or 357 and 370 cm^{-1} in garavellite, from the large peak at 353 to 346 cm^{-1}, attributed to the symmetrical stretching. On the other hand, Bi-S bonds should vibrate at a much slower rate than Sb–S and downshift their frequencies — such a trend is obvious at 353, 349 and 346 cm^{-1} for berthierite, Bi-berthierite and garavellite, respectively, likely linked to increasing Bi-substitution in this direction. The effect of the higher mass of bismuth probably combines with increasing interatomic distances, which are 2.774 Å and 2.818 Å for $(Sb2–S)_{ber}$ (Lukaszewicz et al. 2001) and $(Bi–S)_{gar}$ (Bindi & Menchetti 2005), respectively. For this reason, the peak at 346 cm^{-1}, regarded by Kharbish & Andráš (2014) as the antisymmetrical stretching, may still be attributed to the $\nu 1$ symmetric stretching mode. Generally, this high-frequency domain is marked by downshifts, possibly pointing to the prevailing influence of the mass of Bi atom over shortening of Sb1–S distances. For the more precise band assignment and interpretation of the vibrational spectra of this type of mineral with complex structure, polarized Raman measurements would be necessary.

The complex evolution of the Strieborná vein contains various mineralogical stages where the siderite stage is older than the quartz–sulphidic stage. Proposals for the siderite formation are fairly different. Žák et al. (1991) and Radvanec et al. (2004) connect the veins with the hydrothermal circulation of metamorphic fluids which were probably mixed with meteoric waters leaching Permian evaporites. This model supposes the Variscan mineralization phase to be dominant and the Alpine one less important. A completely different view is offered by Hurai et al. (1998, 2002), presuming the siderite mineralization in the Gemeric area to be formed from basinal brines expelled during compression, linked to a continental collision of the Alpine Orogeny. Several (at least two)

Table 5: Electron microprobe analyses of tintinaite and kobellite with calculated N. N (homologue number) was calculated from the microprobe analyses by the following equation (Zakrzewski & Makovicky 1986): $N = x(6M^{2+} + 3M^{3+})/(4M^{3+} - M^{2+}) + (1-x)(5M^{2+} + 2M^{3+})/(4M^{3+} - M^{2+})$, where $x = T^{+}/(T^{+} + T^{2+})$, $(1-x) = T^{2+}/(T^{+} + T^{2+})$ and T^{+} is content of Cu, T^{2+} is content of divalent cations (Fe), M^{2+} is sum of divalent "large" cations (Pb) and M^{3+} is sum of trivalent "large" cations (Sb+Bi). Ag content was divided to M^{2+} and M^{3+} through "lillianite substitution" Ag+Bi=2Pb. H.n. — horizon number.

Sample	h.n.	Ag	Fe	Sb	Hg	Bi	Cu	S	Pb	Total	
RV 2753	6	0.05	0.04	20.64	0.67	19.90	2.44	19.39	36.41	99.52	
4 RV-Z-1	6	0.17	0.03	22.53	0.59	18.61	2.26	19.76	36.28	100.24	
4 RV-Z-1	6	0.00	0.06	19.19	0.29	22.11	2.22	19.11	36.87	99.92	
4 RV-Z-1	6	0.04	0.22	18.74	0.86	21.74	2.11	18.82	36.35	99.00	
4 RV-Z-1	6	0.19	0.06	21.30	0.42	20.29	2.44	19.12	35.43	99.26	
4 RV-Z-1	6	0.18	0.05	22.62	0.73	18.18	2.24	19.48	35.44	98.91	
4 RV-Z-1	6	0.22	0.06	25.24	0.63	14.95	2.22	19.73	35.88	98.92	
4 RV-Z-1	6	0.25	0.05	24.51	0.56	16.18	2.32	19.49	34.98	98.33	
103-446	10	0.17	0.09	14.42	0.55	30.19	2.18	18.63	33.84	100.08	
103-446	10	0.09	0.11	14.58	0.63	29.79	2.20	18.62	34.54	100.56	
103-446	10	0.07	0.39	15.06	0.87	28.57	2.00	18.63	34.32	99.91	
4 RV-Z-1	6	0	0.38	11.63	0.26	32.73	1.87	18.21	34.87	99.95	
4 RV-Z-1	6	0	0.44	11.58	0.18	32.42	1.78	18.27	35.07	99.73	
4 RV-Z-1	6	0	0.37	11.55	0.11	33.21	1.76	18.18	34.70	99.88	
Formula calculated to sum Pb+Sb+Bi+Ag=26										Sb/Sb+Bi	N
RV 2753	6	0.03	0.04	9.81	0.19	5.51	2.22	35.01	10.17	0.64	2.08
4 RV-Z-1	6	0.09	0.03	10.53	0.17	5.07	2.02	35.07	9.96	0.68	2.03
4 RV-Z-1	6	0.00	0.06	9.23	0.08	6.20	2.05	34.90	10.42	0.60	2.11
4 RV-Z-1	6	0.02	0.23	9.12	0.25	6.16	1.97	34.76	10.39	0.60	2.08
4 RV-Z-1	6	0.10	0.06	10.18	0.12	5.65	2.23	34.68	9.94	0.64	1.99
4 RV-Z-1	6	0.09	0.05	10.71	0.21	5.02	2.03	35.02	9.86	0.68	1.99
4 RV-Z-1	6	0.11	0.06	11.78	0.18	4.07	1.98	34.97	9.84	0.74	1.98
4 RV-Z-1	6	0.13	0.05	11.55	0.16	4.44	2.10	34.87	9.69	0.72	1.94
103-446	10	0.09	0.10	7.12	0.16	8.69	2.06	34.93	9.82	0.45	1.97
103-446	10	0.05	0.12	7.18	0.19	8.55	2.08	34.84	10.00	0.46	2.00
103-446	10	0.04	0.42	7.42	0.26	8.20	1.89	34.84	9.93	0.48	1.94
4 RV-Z-1	6	0.00	0.42	5.87	0.08	9.62	1.80	34.87	10.33	0.38	2.01
4 RV-Z-1	6	0.00	0.48	5.84	0.05	9.53	1.72	34.98	10.40	0.38	2.01
4 RV-Z-1	6	0.00	0.41	5.84	0.03	9.78	1.70	34.90	10.31	0.37	1.99

Table 6: Electron microprobe analyses of tetrahedrite (*n* is average of 90 analyses). H.no. — horizon number).

Sample	h. no.	Ag	Fe	Sb	Hg	As	Bi	Cu	S	Zn	Cd	Total
RV 2750	6	0.88	5.55	28.63	1.42	0.39	0.32	36.98	24.86	0.82	0.03	99.91
RV 2753	6	1.31	5.38	28.63	1.87	0.17	0.40	37.19	24.87	0.77	0.16	100.75
5RV-5-SOS	6	1.00	5.92	29.59	1.10	0.04	0.20	37.49	24.75	0.57	0.08	100.74
5RV-5-SOS	6	0.84	5.56	28.43	1.51	0.48	0.03	37.81	24.71	0.59	0.11	100.06
1 RV-Z-2	6	0.91	5.91	28.88	1.15	0.41	0	37.30	24.64	0.66	0.10	99.96
1 RV-Z-2	6	0.87	5.78	28.94	0.99	0.37	0	37.21	24.31	0.66	0.06	99.18
n = 90		*0.90*	*5.52*	*28.38*	*1.18*	*0.61*	*0.09*	*37.50*	*24.72*	*0.87*	*0.05*	*99.87*
Formula based on 29 apfu												
RV 2750	6	0.14	1.67	3.95	0.12	0.09	0.03	9.77	13.02	0.21	0.01	
RV 2753	6	0.20	1.61	3.94	0.16	0.04	0.03	9.80	12.99	0.20	0.02	
5RV-5-SOS	6	0.15	1.77	4.06	0.09	0.01	0.02	9.85	12.89	0.15	0.01	
5RV-5-SOS	6	0.13	1.67	3.91	0.13	0.11	0.00	9.97	12.91	0.15	0.02	
1 RV-Z-2	6	0.14	1.77	3.98	0.10	0.09	0.00	9.84	12.88	0.17	0.02	
1 RV-Z-2	6	0.14	1.75	4.02	0.08	0.08	0.00	9.91	12.83	0.17	0.01	
n = 90		*0.14*	*1.66*	*3.91*	*0.10*	*0.14*	*0.01*	*9.89*	*12.92*	*0.22*	*0.01*	

quartz–sulphidic mineralization stages containing two tetrahedrite generations appear to be markedly younger compared to the siderite mineralization (Mesarčík et al. 1991; Sasvári & Maťo 1998). In our study, tetrahedrite fills tension joints and tension irregular segments within deformed vein boudine structures (Fig. 2). Typically, tetrahedrite from the Gemeric Superunit has a low Bi content (e.g., Pršek & Biroň 2007; Števko et al. 2015). In the Strieborná vein the last two mineralogical stages (older and younger sulphosalts associations) are documented from all mine levels where sulphosalts appear exclusively in apical parts of the vein body. The garavellite relation to tetrahedrite is marked by the corrosion edges of minerals of the berthierite–garavellite series which most probably originated after the tetrahedrite mineralization by a late hydrothermal solution probably enriched in Bi and Sb.

It was possible to determine the vertical zonality of sulphosalts (i.e. Sb, Ag decrease and *vs.* Bi increase with depth) in the Strieborná vein. Sb-enriched phases of the younger sulphosalt association (chalcostibite–stibnite–berthierite) were not found deeper than the 10th mine horizon. In contrast, the older sulphosalt association (tintinaite–kobellite–Bi-jamesonite–bournonite) is more abundant on deeper mining levels. The typical feature of the berthierite–garavellite series is its linkage to tetrahedrite nests above the 10th mine level. The presence of Sb (the younger sulphosalts stage) in the vein body has been observed only in apical vein parts located in metasandstones and metapelites between the 6th and 8th mining levels. Garavellite –berthierite and other sulphosalts are not present on the 10th mine level hosted in metavolcanic rocks. The multiple tectonometamorphic reprocessing of the vein body in the shear zone also

facilitates ascent of hydrothermal fluids to rheologically contrasting environments. The association of the tintinaite–kobellite series (with Bi>Sb) — Bi-jamesonite belongs to the end of the first sulphidic mineralization stage which is typical for the entire Gemeric Superunit. Later on, the older sulphosalt stage was overprinted by a younger one with the increased Sb content**.** Berthierite–garavellite series and stibnite–bismuthinite series were formed together. This stage corresponds to the younger quartz–stibnite stage (Varček 1985; Hurai et al. 2008) which is well documented in nearby Sb deposits of the so called "stibnite belt" in the Gemeric unit, ranging from Betliar to Zlatá Idka (e.g., Klimko et al. 2009; Pršek & Lauko 2009).

The source of increased Sb content in the fluids responsible for the formation of the younger sulphosalt association could be related to the remobilization or development of the nearby Sb deposit in Čučma. Beside the sulphosalt associations, the vein filling of the Strieborná also contains at least two generations of arsenopyrite, pyrite and quartz. The outlined succession scheme in Figure 4 reflects the multi-stage evolution of the quartz-sulphidic mineralization. We assume that different parageneses could reflect structural events in the shear zone, which are also responsible for the complicated morphology of the Strieborná vein and other veins in the Rožňava ore field.

Table 7: Electron microprobe analyses of chalcostibite and Bi-chalcostibite (sample PJ-5B, no. 26, 27, 28). *N* is average of 10 analyses. H.no. — horizon number.

Sample	h.no.	Ag	Fe	Sb	Hg	As	Bi	Cu	S	Total
RV 2750	6	0.02	0.87	49.19	0	0.02	0	24.84	25.10	100.04
RV 2750	6	0	0.90	49.02	0.02	0.13	0.10	24.99	25.15	100.32
RV 2750	6	0.02	0.39	47.28	0.07	0.01	1.78	25.34	24.93	99.90
RV 2750	6	0.01	0.60	45.52	0.07	0.10	2.36	25.15	25.64	99.46
RV 2750	6	0.03	0.36	47.68	0	0	0.34	25.58	24.87	98.87
n=10		*0.02*	*0.78*	*48.15*	*0.03*	*0.06*	*1.04*	*24.72*	*25.33*	*100.17*
PJ-5B	8	0.01	0.11	36.15	0	0.15	14.3	24.20	24.8	99.00
PJ-5B	8	0	0.09	36.72	0	0.02	15.9	24.41	24.21	100.53
PJ-5B	8	0	0.16	36.37	0	0.02	15.46	24.17	23.89	100.01
Formula calculated to sum Sb+Cu+Bi=2										
RV 2750	6	0.00	0.04	1.01	0.00	0.00	0.00	0.98	1.96	
RV 2750	6	0.00	0.04	1.01	0.00	0.00	0.00	0.98	1.96	
RV 2750	6	0.00	0.02	0.98	0.00	0.00	0.02	1.01	1.97	
RV 2750	6	0.00	0.03	0.94	0.00	0.00	0.03	0.99	2.01	
RV 2750	6	0.00	0.02	0.99	0.00	0.00	0.00	1.02	1.97	
n=10		*0.00*	*0.04*	*0.99*	*0.00*	*0.00*	*0.01*	*0.98*	*1.98*	
PJ-5B	8	0.00	0.01	0.79	0.00	0.01	0.18	1.01	2.00	
PJ-5B	8	0.00	0.00	0.80	0.00	0.00	0.19	1.01	1.99	
PJ-5B	8	0.00	0.01	0.80	0.00	0.00	0.20	1.01	1.98	

Table 8: Electron microprobe analyses of antimonite, antimonite–bizmuthinite solid solution ("horobetsuite") and bizmuthinite. H.no. — horizon number.

Sample	h.no.	Fe	Sb	Bi	Cu	S	Pb	Total
RV 2750	6	0.46	70.51	0	1.13	28.13	0	100.21
RV 2750	6	0.59	70.34	0.07	0.33	27.62	0.10	99.09
5 RV-5	6	0.84	62.70	8.17	0.06	27.12	0.64	99.65
RV 2750	6	0.71	38.84	35.82	1.31	23.78	0.07	100.52
RV 2754	6	1.45	37.82	36.07	1.31	23.55	0.30	100.54
RV 2754	6	1.65	37.29	35.53	1.73	23.11	0.18	99.54
RV 2750	6	0.72	32.70	43.25	1.12	22.48	0.14	100.43
RV 2754	6	0.19	16.48	59.21	1.80	20.38	0.11	98.26
RV 2754	6	0.18	15.27	63.94	1.14	20.87	0.16	101.56
5 RV-5	6	0.34	11.64	67.76	0.18	21.80	0	101.00
S-3B	8	0.17	6.58	74.86	0.15	19.83	0	101.58
4 RV-Z-1	6	0.06	0.29	81.03	0.49	18.57	0.35	100.76
Formula calculated to sum Sb + Cu + Bi = 2								
RV 2750	6	0.03	1.95	0.00	0.06	2.96	0.00	
RV 2750	6	0.04	1.98	0.00	0.02	2.96	0.00	
5 RV-5	6	0.05	1.81	0.14	0.00	2.97	0.01	
RV 2750	6	0.05	1.26	0.68	0.08	2.93	0.00	
RV 2754	6	0.10	1.23	0.68	0.08	2.90	0.01	
RV 2754	6	0.12	1.22	0.68	0.11	2.87	0.00	
RV 2750	6	0.05	1.11	0.86	0.07	2.90	0.00	
RV 2754	6	0.02	0.62	1.30	0.13	2.92	0.00	
RV 2754	6	0.01	0.57	1.39	0.08	2.95	0.00	
5 RV-5	6	0.03	0.44	1.49	0.01	3.02	0.00	
S-3B	8	0.01	0.26	1.73	0.01	2.98	0.00	
4 RV-Z-1	6	0.01	0.01	1.98	0.04	2.95	0.01	

Conclusions

The hydrothermal siderite and younger quartz–sulphide mineralization in the Strieborná vein was related to hydrothermal activity along the Transgemeric shear zone during Cretaceous. The sulphide mineralization is dominated by sulphosalts, the berthierite–garavellite series. This study has determined compositional changes of this series with depth and has confirmed the first complete continuous series from berthierite ($Fe_{1.0}Sb_{1.98}S_{3.98}$) to garavellite ($Fe_{0.97}Sb_{1.06}Bi_{0.91}S_{4.01}$) through the Bi-berthierite in the Western Carpathians and worldwide. The two sulphosalt stages include early association of tintinaite–kobellite series — Bi-jamesonite –bournonite–tetrahedrite and the later association formed by chalcostibite–berthierite–garavellite series — "horobetsuite" (Bi-stibnite, Sb-bismuthinite)–native Bi-stibnite.

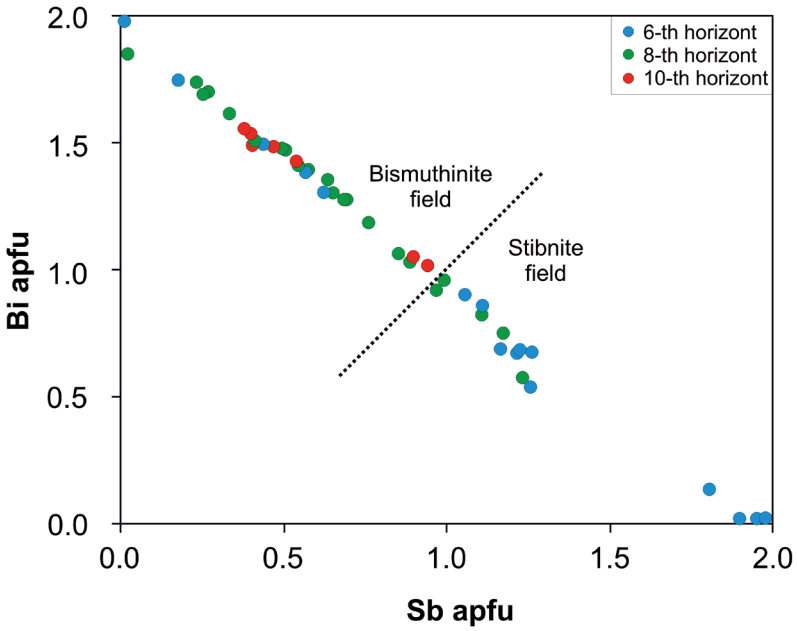

Fig. 11 Sb vs. Bi (apfu) plot for members of the bismuthinite–stibnite solid solution from the Strieborná vein. Dashed line represents formal border between bismuthinite and stibnite.

Table 9: Electron microprobe analyses of ullmanite. H.no. (horizon number).

Sample	h.no.	Fe	Sb	As	Cu	Ni	S	Total
1 RV-Z-2	6	0.90	56.49	1.48	0.18	26.37	14.60	100.01
1 RV-Z-2	6	1.29	56.76	1.14	0.05	26.32	15.05	100.59
S-3B	8	0.14	56.95	0.88	0	26.67	14.93	99.57
S-3B	8	0.23	56.62	0.87	0	26.60	15.02	99.33
Formula based on 2 cations								
1 RV-Z-2	6	0.03	0.99	0.04	0.01	0.96	0.97	
1 RV-Z-2	6	0.05	0.98	0.03	0.00	0.95	0.99	
S-3B	8	0.01	1.00	0.03	0.00	0.97	1.00	
S-3B	8	0.01	0.99	0.02	0.00	0.97	1.00	

The chemistry of sulphosalts changes with depth: the antimony content decreases while Bi content increases.

The Raman spectra were obtained and interpreted for representative phases (berthierite, Bi-berthierite and garavellite). The Raman spectroscopy revealed the peak shifts that depend on an elemental substitution and helped link the equivalent peaks of garavellite and berthierite through Bi-berthierite.

Acknowledgements: We are thankful to the handling editor Dr. Peter Koděra and anonymous reviewers for constructive critical comments which helped to improve the MS. This work was financially supported by the VEGA project (2/0023/17) and by the Operational Programme Research and Development through the projects ITMS: 26220120064 and ITMS: 26210120013, which have been co-financed through the European Regional Development Fund.

References

Andráš P., Jeleň S. & Caňo F. 1993: Bismuth ore mineralization in the Pezinok deposit (western Slovakia). *Mineralia Slovaca* 25, 221–223 (in Slovak).

Bindi L. & Menchetti S. 2005: Garavellite, $FeSbBiS_4$, from the Caspari mine, North Rhine-Westphalia, Germany: composition, physical properties and determination of the crystal structure. *Mineral. Petrol.* 85, 131–139.

Borovikov A.A., Paľchik L.N. & Pospelova L.N. 1990: New bismuth-bearing variety of berthierite. *Geologiya i Geofizika* 31, 130–135 (in Russian).

Buerger M.J. & Hahn T. 1954: The crystal structure of berthierite, $FeSb_2S_4$. *Am. Mineral.* 39, 319–319.

Ciobanu C.L., Brugger J., Cook N.J., S.J., Elliott P., Damian G. & Damian F. 2014: Graţianite, $MnBi_2S_4$, a new mineral from the Băiţa Bihor skarn, Romania. *Am. Mineral.* 99, 1163–1170.

Dianiška I. 2013: Partial report with reserves calculation of Rožňava deposit — Silver vein — status as of June 30, 2013. *Open file report, Manuscript archive, Geol. prieskum, š.p.*, Spišská Nová Ves, 1–140.

Eisele G. 1907: Gömör and Malohont legally united counties of mining. *Monograph,* Selmecz-bánya, 1–185.

Ferenc Š. & Dzúrová M. 2015: Mineral phases of the berthierite-garavellite series from the Klenovec-Medené occurrence (Slovenské Rudohorie Mts. — Veporic Unit), Slovak Republic. *Ageos* 7, 29–36.

Gregorio F., Lattanzi P. & Tanelli G. 1979: Garavellite $FeSbBiS_4$, a new mineral from the Cu-Fe deposit of Valle del Frigido in the Apuane Alps, northern Tuscany, Italy. *Geol. Mag.* 43, 99–102.

Herčko I. 1971: Antimony ore mining in Slovakia between 1926–1945. *Rudy* 19, 119–122.

Hurai V., Gazdačko Ľ., Ferenčíková E., Majzlan J. & Repčok I. 1998: Origin of ore-forming fluids of the vein siderite deposits Gretla, Jedľovec and Rudňany (Spišsko-gemerské Rudohorie Mts.). *Mineralia Slovaca* 30, 423–430 (in Slovak).

Hurai V., Harčová E., Huraiová M., Ozdín D., Prochaska W. & Wiegerová V. 2002: Origin of siderite veins in the Western Carpathians I. *P–T–X–*δ^{13}C–δ^{18}O relations in ore-forming brines of the Rudňany deposits. *Ore Geol Rev.* 21, 67–101.

Hurai V., Lexa O., Schulmann K., Montigny R., Prochaska W., Frank W., Konečný P., Kráľ J., Thomas R. & Chovan M. 2008: Mobilization of ore fluids during Alpine metamorphism: evidence from hydrothermal veins in the Variscan basement of Western Carpathians, Slovakia. *Geofluids* 8, 3, 181–207.

Chovan M., Majzlan J., Ragan M., Siman P. & Krištín J. 1998: Pb–Sb and Pb–Sb–Bi sulphosalts and associated sulphides from Dúbrava antimony deposit, Nízke Tatry Mts. *Acta Geol. Univ Comen.* 53, 37–49.

Kharbish S. & Andráš P. 2014: Investigations of the Fe sulfosalts berthierite, garavellite, arsenopyrite and gudmundite by Raman spectroscopy. *Mineral. Mag.* 78, 5, 1287–1299.

Klimko T., Chovan M. & Huraiová M. 2009: Hydrothermal mineralization of stibnite veins in the Spiš-Gemer Ore Mts. *Mineralia Slovaca* 41, 115–132 (in Slovak).

Kroumova E., Aroyo M.I., Perez Mato J.M., Kirov A., Capillas C., Ivantchev S. & Wondratschek H. 2003: Bilbao Crystallographic Server: useful databases and tools for phase transitions studies. *Phase Transitions* 76, 1–2, 155–170.

Kupčík V., Schneider A. & Varček C. 1969: Chemismus von einigen Bi sulfosalzen aus dem Zips-Gömörer Erzgebirge (CSSR). *Neues Jahrb. Mineral*., *Monatsh.* 445–454.

Lafuente B., Downs R.T., Yang H. & Stone N. 2015: The power of databases: the RRUFF project. In: Armbruster T. & Danisi R.M. (Eds.): Highlights in Mineralogical Crystallography. *W. De Gruyter*, Berlin, 1–30.

Lemoine P.P., Carre D. & Robert F. 1991: Structure du Sulfure de Fer et d'Antimoine, $FeSb_2S_4$ (berthiérite). *Acta Crystallogr.* 47, 938–940.

Lexa O., Schulmann K. & Ježek J. 2003: Cretaceous collision and indentation in the West Carpathians: View based on structural analysis and numerical modeling. *Tectonics* 22, 6, 1066.

Li J., Zhang G. & Zuo F. 1998: Experimental study on a paragenetic association of antimony-bismuth sulfosalt minerals and the synthesis of berthierite-garavellite series. *Acta Mineral. Sinica* 18, 119–125.

Liu J., Liu J., Li J., Xie H., Wang J., Deng J., Feng C., Qi F. & Zhang N. 2008: Experimental synthesis of the stibnite-antimonselite solid solution series. *Int. Geol. Rev.* 50, 2, 163–176.

Litochleb J., Krištín J. & Šrein V. 1990: Bismuth minerals of the Au-bearing mineralization from Kasejovice (SW Bohemia). *Věstník Ústředního ústavu geologického*, 65, 279–289 (in Czech).

Lukaszewicz K., Pietraszko A., Stepien-Damm J., Kajokas A., Grigas J. & Drulis H. 2001: Crystal structure, Mössbauer spectra, thermal expansion, and phase transition of berthierite $FeSb_2S_4$. *J. Solid State Chem.* 16, 2, 79–83.

Majzlan J. & Chovan M. 1997: Hydrothermal mineralization in the Mlynná dolina valley, Nízke Tatry Mts. *Mineralia Slovaca* 29, 149–158 (in Slovak).

Makreski P., Petruševski G., Ugarković S. & Jovanovski G. 2013: Laser-induced transformation of stibnite (Sb_2S_3) and other structurally related salts. *Vibrational Spectroscopy*, 68, 177–182

Maťo Ľ. & Sasvári T. 1997: Golden tetrahedrite of the Silver vein (Mária mine), Rožňava. *Mineralia Slovaca* 29, 3, 237–239.

Mesarčík I., Švantnerová E., Zatroch P., Bachňák M., Jeleň M., Leška S., Hajči T., Palčo A., Tuček Ľ., Košuth M., Ujpál Z., Marko F. & Stupák J. 1991: The Rožňava-Strieborná vein II., Fe, Cu, Ag ore — Reserve estimation, Final report. *Open file report, Manuscript archive, Geofond,* Bratislava, 1–120 (in Slovak).

Mesarčík I. 1994: Preliminary report with operational reserves calculation of the Rožňava–Silver vein II. *Open file report, Manuscript archive, Geoenvex, s.r.o.*, Rožňava, 1–32.

Moëlo Y., Makovicky E., Mozgova N.N., Jambor J.L., Cook N., Pring A., Paar W., Nickel E., Graeser S., Karup-Møller S., Balić-Žunić T., Mumme W.G., Vurro F., Topa D., Bindi L., Bente K. & Shimizu M. 2008: Sulfosalt systematics: a review report of the sulfosalt sub-committee of the IMA commission on ore mineralogy. *Eur J Mineral*, 20, 7–46.

Orlandi P., Moëlo Y. & Biagioni C. 2010: Lead-antimony sulfosalts from Tuscany (Italy). Dadsonite from the Buca della Vena mine and Bi-rich izoklakeite from the Seravezza marble quarries. *Periodico di Mineralogia* 79, 1, 113–121.

Papp K. 1915: The Hungarian empire iron ore and coal reserves. *Franklin-Társulat nyomdája*, Budapest, 1–725.

Pavlík E. 1967: 20-th years of the Iron-ore mines Spišská NováVes. *Zbor. Slov. ban. Múz. Banská Štiavnica* 3, 103–115.

Pršek J. & Biroň A. 2007: Jaskólskiite and associated sulphosalts from Aurélia vein, Spišsko-gemerské rudohorie Mts. *Mineralia Slovaca* 39, 141–146 (in Slovak).

Pršek J. & Mikuš T. 2006: Bi sulphosalts from the Ľubietová–Kolba occurrence. *Mineralia Slovaca* 38, 159–164 (in Slovak).

Pršek J. & Lauko Ľ. 2009: Hydrothermal vein mineralization at Zlatá Idka (Spiš–Gemer Ore Mts.) *Mineralia Slovaca* 41, 133–150 (in Slovak).

Radvanec M., Grecula P. & Žák K. 2004: Siderite mineralization of the Gemericum Superunit (Western Carpathians, Slovakia): review and a revised genetic model. *Ore Geol Rev*. 24, 267–298.

Sasvári T. & Maťo Ľ. 1998: The characteristics of the Rožňava ore district, in relation to the structural-tectonic analysis and mineralization exampled by the deposition conditions of the Strieborná vein, Mária mine, Rožňava. *Acta Mont. Slovaca*, *Monograph. — Rožňava ore field*, 3, 1, 33–117.

Schifter F. 1938: Iron-ore mining in the Spiš–Gemer Ore Mountains. *Sbor. Spoj. ban. revíru Slov. Podkarpat. Rus* 1, 56–167.

Števko M., Sejkora J. & Peterec D. 2015: Grumiplucite from the Rudňany deposit, Slovakia: a second world-occurrence and new data. *J. Geol. Sci*. 60, 269–281.

Uher P., Michal S. & Vitáloš J. 2000: The Pezinok Antimony Mine: Malé Karpaty Mountains, Slovakia. *Mineral Record* 31, 2, 153–162.

Varček C. 1985: Metalogenesis of Spiš – Gemer Ore Mts. and Rudňany ore field characteristic. In: Cambel B. & Jarkovský J. (Eds.): Rudňany ore field. Geochemical and metalogenetic characteristic. *Veda*, Bratislava, 61–77.

Wang A., Han J., Guo L., Yu J. & Zeng P. 1994: Database of standard Raman spectra of minerals and related inorganic crystals. *Applied Spectroscopy* 48, 959–968.

Wei B., Li S., Yin Z. & Geng M. 1985: The discovery of the native bismuth-antimony system minerals and garavellite. *Shaanxi Dizhi* 3, 31–37 (in Chinese).

Zakrzewski M. & Makovický E. 1986: Izoklakeite from Vena, Sweden, and kobellite homologous series. *Can. Mineral*. 24, 7–18.

Žák K., Radvanec M., Grecula P. & Bartalský B. 1991: Sr, S, C, O isotopes and metamorphic–hydrothermal model of vein mineralization, Gemeric Unit, Western Carpathians. *Mineralia Slovaca* 23, 95–108 (in Slovak).